



**UNIVERSITI PUTRA MALAYSIA**

**STUDIES ON GIANT AND COLOSSAL MAGNETORESISTANCE OF  
ALLOY AND CERAMIC PREPARED BY RF MAGNETRON  
SPUTTERING AND PULSED LASER ABLATION TECHNIQUES**

**LIM KEAN PAH**

**FSAS 2002 56**

**STUDIES ON GIANT AND COLOSSAL MAGNETORESISTANCE OF  
ALLOY AND CERAMIC PREPARED BY RF MAGNETRON  
SPUTTERING AND PULSED LASER ABLATION TECHNIQUES**

**By**

**LIM KEAN PAH**

**Thesis Submitted to the School of Graduate Studies, Universiti Putra Malaysia,  
in Fulfillment of the Requirement for the Degree of Doctor of Philosophy**

**November 2002**



Abstract of thesis presented to the Senate of Universiti Putra Malaysia in fulfillment of the requirements for the degree of Doctor of Philosophy

**STUDIES ON GIANT AND COLOSSAL MAGNETORESISTANCE OF  
ALLOY AND CERAMIC PREPARED BY RF MAGNETRON  
SPUTTERING AND PULSED LASER ABLATION TECHNIQUES**

**By**

**LIM KEAN PAH**

**November 2002**

**Chairman : Professor Abdul Halim Shaari, Ph.D.**

**Faculty : Science and Environmental Studies**

Magnetic thin films based on the giant magnetoresistance (GMR) and colossal magnetoresistance (CMR) effects are currently being used as head sensor in the magnetic data storage technology. With the technological revolution in the magnetic recording world of last decades, a need of better and more sensitive magnetoresistance material arises for head sensing. In the first part of this work, a series of Ag-Fe-Co granular films with different composition and thickness had been fabricated onto microscope glass slides using RF magnetron sputtering system. The crystalline analysis show that the as-deposited films consist of  $\langle 111 \rangle$  and  $\langle 200 \rangle$  silver texture. Negative GMR values have been obtained and no tendency to saturate at any temperature has been observed. The experimental results show that the GMR value is governed by the composition, microstructure, thickness and temperature. Under an optimum condition, formation of the right shape and size of magnetic cluster in the matrix will cause rapid increase of the GMR value. In this work, the optimum conditions for the highest GMR value of 7.6% measured at room

temperature is obtained for the  $Ag_{87.0}Fe_{9.5}Co_{3.5}$  deposited for 60 minutes. In the second part of the work, Pulsed Laser Deposition (PLD) system had been assembled to fabricate ceramic films. Surface studies of the laser irradiated targets show that low fluence of laser causes the periodic structure such as ripples, ridges and cone. However, high fluence of laser will cause the exfoliation and hydrodynamic sputtering process. In this work, bulk and thin films of  $La_{0.67}Ca_{0.33}MnO_3$  (LCMO),  $La_{0.67}Sr_{0.33}MnO_3$  (LSMO) and  $La_{0.67}Ba_{0.33}MnO_3$  (LBMO) had been prepared. Scanning electron microscope micrograph shows that the films consist of wide range of small particles size distribution and they are in spherical shape. The XRD shows that the as-deposited film is in amorphous state and later transfers to polycrystalline state when heat-treatment is applied. Curie temperature,  $T_c$  of the films is slightly lower than that of bulk due to the existing amorphous or antiferromagnetic phases at the grain boundaries (GBs). However, the resistances show a huge increase due to the existence of the insulating GBs region. Overall, negative CMR had been obtained for bulk and film samples. The CMR value of polycrystalline films increases with decreasing temperature at low applied magnetic field. This behaviour, which is known as Low Field Magnetoresistance (LFMR), is expected to be due to the polarization of electrons in the magnetically disordered regions near the grain boundaries.

Abstrak tesis yang dikemukakan kepada Senat Universiti Putra Malaysia sebagai memenuhi keperluan untuk ijazah Doktor Falsafah

**KAJIAN TENTANG MAGNETORINTANGAN GERGASI DAN RAKSAKSA  
BAGI ALOI DAN CERAMIK YANG DISEDIAKAN MELALUI PERCIKAN  
MAGNETRON RF DAN TEKNIK MENDAPAN PULSE LASER**

**Oleh**

**LIM KEAN PAH**

**November 2002**

**Pengerusi : Profesor Abdul Halim Shaari, Ph.D.**

**Fakulti : Sains dan Pengajian Alam Sekitar**

Saput nipis magnet yang berdasarkan kesan magnetorintangan gergasi (MRG) dan magnetorintangan raksaksa (MRR) kini telah diguna sebagai kepala sensor dalam teknologi data simpanan bermagnet. Dengan revolusi teknologi dalam dunia pengrekodan bermagnet pada dekat yang lepas, keperluan bahan magnetorintangan yang lebih baik dan peka diperlukan bagi kepala sensor. Dalam bahagian pertama kerja ini, satu siri saput granular Ag-Fe-Co telah disediakan di atas slid kaca mikroskop pada ketebalan dan komposisi yang berbeza dengan menggunakan sistem percikan magnetron RF. Pencirian hablur menunjukkan bahawa saput nipis baru mendap mengandungi tekstur perak  $\langle 111 \rangle$  dan  $\langle 200 \rangle$ . Nilai negatif MRG telah didapati dan tiada kesan untuk menjadi tepu dilihat pada mana-mana suhu. Keputusan eksperimen menunjukkan bahawa nilai MRG dikuasai oleh komposisi, mikrostruktur, ketebalan dan suhu. Di bawah keadaan optimum, pembentukan rupa bentuk dan saiz butiran yang betul di dalam saput akan menyebabkan nilai MRG bertambah secara mendadak. Dalam kerja ini, keadaan optimum untuk mendapat

nilai MRG yang paling tinggi yang bernilai 7.6% diukur pada suhu bilik telah diperolehi bagi  $\text{Ag}_{87.0}\text{Fe}_{9.5}\text{Co}_{3.5}$  yang dimendap selama 60 minit. Dalam bahagian kedua bagi kerja ini, sistem Mendapan Dedenyut Laser (MDL) telah dipasang untuk fabrikasi saput tipis seramik. Kajian permukaan bagi bahan yang disinari cahaya laser menunjukkan bahawa sinaran kuasa rendah laser menyebabkan struktur berkala seperti jurang, bukit dan kon. Manakala, sinaran laser yang tinggi akan menyebabkan process percikan “eksfoliasi” dan “hidrodinamik”. Dalam kerja ini, pepejal dan saput nipis bagi  $\text{La}_{0.67}\text{Ca}_{0.33}\text{MnO}_3$  (LCMO),  $\text{La}_{0.67}\text{Sr}_{0.33}\text{MnO}_3$  (LSMO) dan  $\text{La}_{0.67}\text{Ba}_{0.33}\text{MnO}_3$  (LBMO) telah disediakan. Mikrograf pengimbasan mikroskop elektron menunjukkan bahawa saput mengandungi taburan butiran kecil yang berjulat besar dan berbentuk sfera. Data kitalografi menunjukkan bahawa saput baru mendap adalah dalam bentuk amorfus dan akan bertukar ke bentuk polihablur bila diberi rawatan haba. Suhu Curie,  $T_c$  bagi saput tipis adalah rendah sedikit berbanding dengan bahan pepejal disebabkan oleh wujudnya kawasan amorfus dan antiferromagnet di bahagian sempadan butiran (GBs). Walau bagaimanapun, satu peningkatan mendadak pada rintangan berlaku disebabkan oleh wujudnya bahagian penebat di GBs. Secara keseluruhan, MRR negatif telah diperolehi bagi sampel pepejal dan saput tipis. Magnitud MRR bagi saput tipis polihablur meningkat dengan penyusutan suhu pada keadaan medan magnet yang rendah. Tingkahlaku ini, dikenali sebagai magnetorintangan medan rendah (LFMR), adalah dijangkakan dan disebabkan oleh pengutuban elektron dalam bahagian kemagnetan yang tidak tersusun berdekatan dengan sempadan butiran.

## ACKNOWLEDGEMENTS

First of all I would like to express my deep sense of gratitude to my supervisor, Professor Dr. Abdul Halim Shaari, for his constant encouragement, constructive suggestions and continuous discussion throughout the project. I am very grateful to him for giving me the platform to pursue my studies and giving me the opportunity to assemble the first Pulsed Laser Deposition unit in this department. I would like to extend my sincere appreciation to my co-supervisors Associate Prof. Dr. Hishamuddin Bin Zainuddin and Associate Prof. Dr. Chow Sai Pew for their comments, suggestion, guidance and help throughout the research work.

My special thanks to Mr. Ho, Mrs. Azilah, Mrs. Aminah and all the staff from Electron Microscope Unit, Institute of Bioscience for their help in the SEM analysis. Particular thanks are also extended to Miss Siew Siew from Hi-Tech Sdn. Bhd. for her help in getting the high magnification image of the thin film from FESEM. Sincere thanks are due to Mr. Henry from the CLMO for his kind support and help in the cross-section studies.

I would like to thank also my good friends Dr. Noorhana and Mr Woon for their helpful suggestion and encouragement. I am also very thankful to Mr. Razak for his kind technical help and also to other staff in the physics Department who have rendered their help in one way or another throughout the research work. Special thanks also are given to Miss Sim for her help in the XRD analysis.

I am extremely grateful to all my friends Kok, Yu, Kabashi, Dr. Mohamed, Dr. Azhan, Halim, Imad, Iftetan, Yoke Thing, Roy, Soo Fung, Fanny, Jorsophin, Liaw, Teh, Huda, Zolman, Talib, Dr. Rita, Ei Bee and all my friends in UPM who constantly giving encouragements throughout these few years.

The financial support in this work from the Ministry of Science and Technology, under the IRPA vote: 09-02-04-0148 (Fabrication of Magnetoresistive Thin Film having GMR and/or CMR effect as magnetic sensors using Pulsed Laser Ablation) is also gratefully acknowledged. Without this support, it is impossible for us to pursue this project with success. Lastly, I would also like to extend my gratitude to the Malaysian government for granting me the PASCA scholarship.

Last but not least, I would like to give my sincere thanks to all members of my family and my girl friend, Chiu Sze for their love, continuous support, encouragement and understanding.



I certify that an Examination Committee met on 20<sup>th</sup> November 2002 to conduct the final examination of Lim Kean Pah on his Doctor of Philosophy thesis entitled “Studies on Giant and Colossal Magnetoresistance of Alloy and Ceramic Prepared by RF Magnetron Sputtering and Pulsed Laser Ablation Techniques” in accordance with Universiti Pertanian Malaysia (Higher Degree) Act 1980 and Universiti Pertanian Malaysia (Higher Degree) Regulations 1981. The Committee recommends that the candidate be awarded the relevant degree. Members of the Examination Committee are as follows:

**Sidek Abdul Aziz, Ph.D.**

Associate Professor  
Faculty of Science and Environmental Studies  
Universiti Putra Malaysia  
(Chairman)

**Abdul Halim Shaari, Ph.D.**

Professor  
Faculty of Science and Environmental Studies  
Universiti Putra Malaysia  
(Member)

**Hishamuddin Zainuddin, Ph.D.**


Associate Professor  
Faculty of Science and Environmental Studies  
Universiti Putra Malaysia  
(Member)

**Chow Sai Pew, Ph.D.**

Associate Professor  
Faculty of Science and Environmental Studies  
Universiti Putra Malaysia  
(Member)

**Wong Chiow San, Ph.D.**

Professor  
Faculty of Science  
Universiti of Malaya  
(Independent Examiner)



---

**SHAMSHER MOHAMAD RAMADILI, Ph.D.**  
Professor/Deputy Dean  
School of Graduate Studies  
Universiti Putra Malaysia

Date: 20 DEC 2002

This thesis submitted to the Senate of Universiti Putra Malaysia has been accepted as fulfillment of the requirement for the degree of Doctor of Philosophy. The members of the Supervisor Committee are as follows:

**Abdul Halim Shaari, Ph.D.**

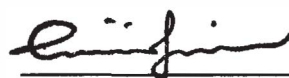
Professor  
Faculty of Science and Environmental Studies  
Universiti Putra Malaysia  
(Chairman)

**Hishamuddin Zainuddin, Ph.D.**

Associate Professor  
Faculty of Science and Environmental Studies  
Universiti Putra Malaysia  
(Member)

**Chow Sai Pew, Ph.D.**

Associate Professor  
Faculty of Science and Environmental Studies  
Universiti Putra Malaysia  
(Member)



---

**AINI IDERIS, Ph.D.**

Professor/Dean  
School of Graduate Studies  
Universiti Putra Malaysia

Date : **13** FEB 2003

## DECLARATION

I hereby declare that the thesis is based on my original work except for quotations and citations which have been duly acknowledged. I also declare that it has not been previously or concurrently submitted for any other degree at UPM or other institutions.



---

(Lim Kean Pah)

Date: 20/12/2002

## Table of Contents

	<b>Page</b>
ABSTRACT	ii
ABSTRAK	iv
ACKNOWLEDGEMENTS	vi
APPROVAL	viii
DECLARATION	x
LIST OF TABLES	xv
LIST OF FIGURES	xvi
LIST OF PLATE	xxiii
LIST OF ABBREVIATIONS/NOTATIONS	xxiv
<b>CHAPTER</b>	
<b>1 GENERAL INTRODUCTION</b>	<b>1.1</b>
1.1 Introduction	1.1
1.2 Objective of Work	1.3
1.3 Thesis Content	1.4
<b>2 LITERATURE REVIEW</b>	<b>2.1</b>
2.1 Introduction	2.1
2.2 Giant Magnetoresistance (GMR) Compounds	2.2
2.2.1 Microstructure Dependence of GMR Value	2.4
2.2.2 Thickness Dependence of GMR Value	2.5
2.2.3 Composition Dependence of GMR Value	2.5
2.2.4 Temperature Dependence of GMR Value	2.6
2.3 Colossal Magnetoresistance (CMR) Compounds	2.6
2.3.1 Manganites Perovskite Properties	2.7
2.3.2 Polycrystalline Manganites Perovskite	2.10
2.3.3 Influence of Heat Treatment of CMR Thin Films	2.13
2.3.4 Substrate Dependence of CMR Thin Films	2.15
2.3.5 Temperature Dependence of CMR Thin Films	2.16
2.3.6 Thickness Dependence of CMR Thin Films	2.17
2.4 Pulsed Laser Deposition	2.18
<b>3 THEORY</b>	<b>3.1</b>
3.1 Thin Film	3.1
3.1.1 Thin Film Growth Process	3.1
3.1.2 Thin film Deposition Techniques	3.2
3.2 Sputtering	3.3
3.2.1 Introduction	3.3
3.2.2 Advantages of Sputtering	3.4
3.2.3 Sputtering Yield and Thresholds	3.5
3.2.4 Glow Discharge	3.5
3.2.5 Mechanism of Sputtering	3.8
3.2.6 Sputtering Deposition	3.9
3.2.7 RF Sputtering	3.9
3.2.8 Magnetron Sputtering	3.10

3.3	Pulsed Laser Deposition System	3.11
3.3.1	Introduction	3.11
3.3.2	Laser and Optical Apertures	3.12
3.3.3	Deposition Chambers	3.13
3.3.4	Target Manipulation	3.15
3.3.5	Substrate Holder and Heaters	3.15
3.3.6	Pumps, Gas Flow and Vacuum Gauges	3.16
3.3.7	Mechanisms of Pulsed Laser Deposition	3.17
3.3.8	Surface Modification of Materials by Laser Irradiation	3.18
	3.3.8.1 Ripples Formation	3.18
	3.3.8.2 Cone Formation	3.19
3.3.9	Advantages of PLD	3.21
3.3.10	PLD Limitation	3.22
3.4	Substrate and Cleaning	3.23
3.5	Magnetoresistance Effects	3.25
3.5.1	Introduction	3.25
3.5.2	Giant Magnetoresistance Effect	3.26
3.5.3	GMR Nanostructure for Multiplayer and Granular Thin Film	3.28
3.5.4	Types of GMR Effects in Multilayer and Granular Thin Film	3.31
3.5.5	A Simple Model of Giant Magnetoresistance	3.32
3.5.6	Giant Magnetoresistance Ratio	3.35
3.5.7	Temperature Dependence of GMR Effect	3.35
3.5.8	Grain Size Dependence of GMR Effect	3.37
3.6	Perovskite Manganites Compounds	3.38
3.6.1	Introduction	3.38
3.6.2	Double exchange (DE)	3.39
3.6.3	Jahn-Teller (JT)	3.40
3.6.4	Tolerance Factor	3.42
3.6.5	Colossal Magnetoresistance (CMR) Effect	3.43
	3.6.5.1 Possible Origin of CMR	3.43
	3.6.5.2 CMR in Polycrystalline Thin Film	3.44
	3.6.5.3 Grain Boundary CMR	3.46
4	METHODOLOGY	4.1
4.1	Radio Frequency Magnetron Sputtering	4.1
4.1.1	Preparing Base Pressure for Sputtering	4.4
4.1.2	Substrate Cleaning	4.4
4.1.3	Thin Film Deposition Process	4.5
4.2	Sample Preparation for CMR bulk samples	4.6
4.2.1	Mixing Homogenous Starting Powder	4.6
4.2.2	Powder Calcinations	4.6
4.2.3	Grinding, Sieving and Pressing Pellets	4.8
4.2.4	Final Sintering	4.8
4.3	Pulsed Laser Deposition (PLD)	4.9
4.3.1	Laser System and Optical System	4.11
4.3.2	Vacuum System	4.14
4.3.3	Deposition Chamber	4.15
4.3.4	Glass Substrate	4.18

4.3.5	Operating Procedures for PLD Deposition	4.18
4.3.6	Samples Cutting and Storage	4.21
4.4	Surface Morphology and Microstructure Studies	4.21
4.5	Cross Section Studies	4.23
4.6	Structures and Phase Identification	4.25
4.7	AC Magnetic Susceptibility Measurement	4.27
4.8	Four Point Probe Resistance Measurements	4.29
4.9	Magnetoresistance Measurement	4.30
4.10	Errors of Measurements	4.33
5	RESULTS & DISCUSSION	5.1
5.1	Ag-Fe-Co Granular Magnetic Thin Film	5.1
5.1.1	Surface Morphology	5.1
5.1.2	Energy Dispersive X-ray (EDX) Analysis	5.3
5.1.3	Microstructure Studies Using X-ray Diffraction Method	5.5
5.1.4	Giant Magnetoresistance Effect	5.10
5.1.5	Deposition Time Dependence of GMR Effect	5.32
5.1.6	Temperature Dependence of GMR Effect	5.38
5.1.7	Composition Dependence of GMR Effect	5.42
5.2	Colossal Magnetoresistance Compound	5.44
5.2.1	Surface Morphology Studies of CMR Pallet	5.45
5.2.2	Surface Morphology Studies of Laser Irradiated Target	5.47
5.2.3	Microstructure Studies of CMR Thin Films	5.51
5.2.4	$\text{La}_{0.67}\text{Ca}_{0.33}\text{MnO}_3$ System	5.60
5.2.4.1	XRD Pattern and Lattice Parameters	5.60
5.2.4.2	Susceptibility and Curie Temperature, $T_c$	5.61
5.2.4.3	Resistance and Phase Transition Temperature, $T_p$	5.62
5.2.4.4	Colossal Magnetoresistance (CMR) Effect	5.64
5.2.5	$\text{La}_{0.67}\text{Sr}_{0.33}\text{MnO}_3$ System	5.70
5.2.5.1	XRD Pattern and Lattice Parameters	5.70
5.2.5.2	Susceptibility and Curie Temperature, $T_c$	5.71
5.2.5.3	Resistance and Phase Transition Temperature, $T_p$	5.72
5.2.5.4	Colossal Magnetoresistance (CMR) Effect	5.73
5.2.6	$\text{La}_{0.67}\text{Ba}_{0.33}\text{MnO}_3$ System	5.81
5.2.6.1	XRD Pattern and Lattice Parameters	5.81
5.2.6.2	Susceptibility and Curie Temperature, $T_c$	5.82
5.2.6.3	Resistance and Phase Transition Temperature, $T_p$	5.83
5.2.6.4	Colossal Magnetoresistance (CMR) Effect	5.85
6	CONCLUSIONS & SUGGESTIONS	6.1
6.1	Conclusions	6.1
6.2	Suggestions	6.6
	REFERENCES	R1
	APPENDICES	
A	Specifications of the 101E Handy YAG laser system.	A1
B	Temperature dependence of AC susceptibility at various applied field and colossal magnetoresistance as a function of applied magnetic field at different temperature for LCMO thin film samples.	A2

C	Temperature dependence of AC susceptibility at various applied field and colossal magnetoresistance as a function of applied magnetic field at different temperature for LSMO thin film samples.	A6
D	Temperature dependence of AC susceptibility for LBMO thin film at various applied field.	A10
E	X-ray Diffraction Pattern (XRD) for the standard peak of pure cobalt (cubic), pure iron (cubic) and pure silver (cubic)	A12
F	Paper Presented and Published in Local and International Conferences	A13
VITA		V1

**LIST OF TABLES**

<b>Tables</b>		<b>Pages</b>
3.1	The colour of luminous zones in glow discharge	3.7
4.1	Experimental parameters during samples fabrication for PLD system	4.20
4.2	Estimated errors of measurements	4.34
5.1	Ag-Fe-Co prepared by RF Magnetron Sputtering System	5.4
5.2	Bulk and thin film samples that have been prepared	5.44



## LIST OF FIGURES

<b>Figures</b>		<b>Pages</b>
2.1	Magnetic phase diagram of the $\text{La}_{1-x}\text{Ca}_x\text{MnO}_3$ system	2.8
2.2	Magnetic phase diagram of the $\text{La}_{1-x}\text{Sr}_x\text{MnO}_3$ system	2.8
2.3	Resistance (a) and magnetoresistance (at $B=1.6\text{T}$ ) (b) versus temperature dependences for LCMO films prepared at identical conditions on different substrate.	2.12
2.4	Temperature dependence of LFMR and the zero-field resistivity for epitaxial LSMO film, polycrystalline LCMO and LSMO films.	2.13
2.5	Temperature dependence of resistivity of $\text{La}_{1-x}\text{MnO}_3$ films grown on various substrates.	2.15
2.6	Magnetoresistance of $\text{La}_{1-x}\text{MnO}_3$ films on various substrates in magnetic field of 0.3 T as a function of temperature.	2.16
2.7	Resistivity as a function of temperature for film of different thickness.	2.18
3.1	Thin film deposition process	3.3
3.2	Luminous zones and dark spaces in a DC glow discharge	3.6
3.3	Physical sputtering process	3.9
3.4	The cross section of a typical RF-cathode including cooling system.	3.10
3.5	The typical set-up for the magnetron sputtering with water-cool system	3.11
3.6	Schematic of the basic thermal cycle induced by a laser pulse	3.19
3.7(a)	Low magnification SEM micrograph of a track produced in a rotating YBCO target	3.20
3.7(b)	High magnification views of cone structures produced in a rotating YBCO target	3.20

3.7(c)	Transition region between cones and ripples	3.21
3.8(a)	GMR nanostructure and their magnetoresistance behaviour for antiferromagnetically coupled multilayer	3.30
3.8(b)	GMR nanostructure and their magnetoresistance behaviour for granular thin film	3.30
3.9(a)	Schematic of conduction in multilayer magnetic thin film and the equivalent resistor network for the antiparallel coupling	3.33
3.9(b)	Schematic of conduction in multilayer magnetic thin film and the equivalent resistor network for the parallel coupling	3.34
3.10	Schematic diagram of double exchange model	3.40
3.11	A sketch of field splitting the five-fold degenerate atomic 3d levels into lower $t_{2g}$ and higher $e_g$ levels	3.41
3.12	Phase diagram at constant doping $x=0.3$ also a function of tolerance factor	3.43
3.13	Temperature dependence of the low-field MR and the zero-field resistivity for polycrystalline LCMO and LSMO films with 14 $\mu\text{m}$ average grain size	3.46
4.1	A schematic of the pumping system for ESM 100 Edwards Sputtering System	4.2
4.2	Schematic diagram for Pulsed Laser Deposition system	4.10
4.3	Value set at controller vs. output laser power	4.12
4.4	Schematic diagram of the target and substrate holder	4.17
4.5	Disk shape thin film sample cut into rectangular shape	4.21
4.6	EDX spectrum for the thin film sample	4.22
4.7	Sample preparation route for cross-section observation	4.24
4.8	Curie-Weiss law shows the presence of paramagnetic phase	4.29
4.9	Schematic diagram of the magnetoresistance setup	4.31

4.10	Four-point probe holder in MR measurement system	4.33
5.1	EDX spectrum for Ag-Co granular thin film	5.3
5.2	XRD pattern for $\text{Ag}_{90}\text{Fe}_{10}$ samples deposited for 30, 40, 50, 60, 70 and 80 minutes.	5.7
5.3	XRD pattern for $\text{Ag}_{87.0}\text{Fe}_{9.5}\text{Co}_{3.5}$ samples deposited for 30, 40, 50, 60, 70 and 80 minutes.	5.8
5.4	XRD pattern for $\text{Ag}_{82}\text{Fe}_{10}\text{Co}_8$ samples deposited for 30, 40, 50, 60, 70 and 80 minutes.	5.8
5.5	XRD pattern for $\text{Ag}_{80}\text{Fe}_7\text{Co}_{13}$ samples deposited for 30, 40, 50, 60, 70 and 80 minutes.	5.9
5.6	XRD pattern for $\text{Ag}_{75}\text{Fe}_6\text{Co}_{19}$ samples deposited for 30, 40, 50, 60, 70 and 80 minutes.	5.9
5.7	XRD pattern for $\text{Ag}_{66}\text{Co}_{34}$ samples deposited for 30, 40, 50, 60, 70 and 80 minutes.	5.10
5.8	GMR curve as a function of applied magnetic field at various temperature for $\text{Ag}_{90}\text{Fe}_{10}$ granular films deposited for (a) 80 minutes, (b) 70 minutes, (c) 60 minutes, (d) 50 minutes, (e) 40 minutes and (f) 30 minutes	5.16
5.9	GMR curve as a function of applied magnetic field at various temperature for $\text{Ag}_{87.0}\text{Fe}_{9.5}\text{Co}_{3.5}$ granular films deposited for (a) 80 minutes, (b) 70 minutes, (c) 60 minutes, (d) 50 minutes, (e) 40 minutes and (f) 30 minutes	5.19
5.10	GMR curve as a function of applied magnetic field at various temperature for $\text{Ag}_{82}\text{Fe}_{10}\text{Co}_8$ granular films deposited for (a) 80 minutes, (b) 70 minutes, (c) 60 minutes, (d) 50 minutes, (e) 40 minutes and (f) 30 minutes	5.22
5.11	GMR curve as a function of applied magnetic field at various temperature for $\text{Ag}_{80}\text{Fe}_7\text{Co}_{13}$ granular films deposited for (a) 80 minutes, (b) 70 minutes, (c) 60 minutes, (d) 50 minutes, (e) 40 minutes and (f) 30 minutes	5.25
5.12	GMR curve as a function of applied magnetic field at various temperature for $\text{Ag}_{75}\text{Fe}_6\text{Co}_{19}$ granular films deposited for (a) 80 minutes, (b) 70 minutes, (c) 60 minutes, (d) 50 minutes, (e) 40 minutes and (f) 30 minutes	5.28

5.13	GMR curve as a function of applied magnetic field at various temperature for $\text{Ag}_{66}\text{Co}_{34}$ granular films deposited for (a) 80 minutes, (b) 70 minutes, (c) 60 minutes, (d) 50 minutes, (e) 40 minutes and (f) 30 minutes	5.31
5.14	GMR curve as a function of deposition times for $\text{Ag}_{90}\text{Fe}_{10}$ granular films measured at various temperature	5.35
5.15	GMR curve as a function of deposition times for $\text{Ag}_{87.0}\text{Fe}_{9.5}\text{Co}_{3.5}$ granular films measured at various temperature	5.35
5.16	GMR curve as a function of deposition times for $\text{Ag}_{82}\text{Fe}_{10}\text{Co}_8$ granular films measured at various temperature	5.36
5.17	GMR curve as a function of deposition times for $\text{Ag}_{80}\text{Fe}_7\text{Co}_{13}$ granular films measured at various temperature	5.36
5.18	GMR curve as a function of deposition times for $\text{Ag}_{75}\text{Fe}_6\text{Co}_{19}$ granular films measured at various temperature	5.37
5.19	GMR curve as a function of deposition times for $\text{Ag}_{66}\text{Co}_{34}$ granular films measured at various temperature	5.37
5.20	GMR curve as a function of measuring temperature for $\text{Ag}_{90}\text{Fe}_{10}$ granular films at various deposited times	5.39
5.21	GMR curve as a function of measuring temperature for $\text{Ag}_{87.0}\text{Fe}_{9.5}\text{Co}_{3.5}$ granular films at various deposited times	5.40
5.22	GMR curve as a function of measuring temperature for $\text{Ag}_{82}\text{Fe}_{10}\text{Co}_8$ granular films at various deposited times	5.40
5.23	GMR curve as a function of measuring temperature for $\text{Ag}_{80}\text{Fe}_7\text{Co}_{13}$ granular films at various deposited times	5.41
5.24	GMR curve as a function of measuring temperature for $\text{Ag}_{75}\text{Fe}_6\text{Co}_{19}$ granular films at various deposited times	5.41
5.25	GMR curve as a function of measuring temperature for $\text{Ag}_{66}\text{Co}_{34}$ granular films at various deposited times	5.42
5.26	Variation of GMR value with the percentage of silver element in the Ag-Fe-Co granular thin film.	5.43
5.27	Scanning electron micrograph of La-Ca-Mn-O bulk sample	5.45

5.28	Scanning electron micrograph of La-Ba-Mn-O bulk sample.	5.46
5.29	Scanning electron micrograph of La-Sr-Mn-O bulk sample.	5.46
5.30	Surface modification of the rotational target irradiated by low fluence laser.	5.47
5.31	Low magnification (35X) scanning electron micrograph of a track produced in a rotating LBMO target.	5.48
5.32	Higher magnification (150X) showing the transition region between cones (at center) and ripples (at both edge).	5.48
5.33	SEM micrograph of a portion of a rotational target which has gone through exfoliation and hydrodynamic sputtering.	5.49
5.34	Optical micrograph of a sectioned and polished LBMO target with cones that have been formed after irradiated by pulsed laser.	5.50
5.35	Optical micrograph of a sectioned and polished LBMO target with ripple and the undisturbed portion.	5.51
5.36	SEM micrograph of droplets formation on the surface of the deposited film.	5.52
5.37	SEM micrograph of droplets in various shape (a) expelled cluster (b) cone with round tips (c) cone with sharp points.	5.53
5.38	SEM micrograph of the LSMO thin film at magnification of 250X.	5.54
5.39	SEM micrograph of the LCMO thin film at magnification of 3,000X	5.55
5.40	SEM micrograph of the LBMO thin film at magnification of 10,000X	5.55
5.41	SEM micrograph of the LBMO thin film at magnification of 50,000X	5.56
5.42	Scanning electron micrograph of a portion of a sectioned deposited film	5.57
5.43	SEM micrograph of a portion of the static target	5.58

5.44	SEM micrograph of the crack surface after annealing process (Magnification 500X)	5.59
5.45	SEM micrograph of the crack surface after annealing process (Magnification 1,000X)	5.59
5.46	XRD spectrum for LCMO bulk and ICDD standard.	5.66
5.47	XRD spectrum for all LCMO thin film.	5.66
5.48	Thermal dependence of AC susceptibility at H=10 Oe for LCMO thin films deposited at various duration.	5.67
5.49	Inverse AC susceptibility against temperature of LCMO system.	5.67
5.50	The temperature dependence of AC susceptibility for LC <sub>3.5</sub> sample at various applied field.	5.68
5.51	Temperature dependence of resistance for LCMO bulk sample.	5.68
5.52	Temperature dependence of resistance for all LCMO thin film.	5.69
5.53	CMR curve of LC <sub>4.0</sub> thin film as a function of magnetic field at various temperatures.	5.69
5.54	CMR curve of all LCMO thin film as a function of temperature for different deposition times.	5.70
5.55	XRD spectrum for LSMO bulk and ICDD standard.	5.75
5.56	XRD spectrum for all LSMO thin film.	5.76
5.57	Thermal dependence of AC susceptibility at H=10 Oe for all LSMO thin films.	5.76
5.58	Thermal dependence of AC susceptibility at H=10 Oe for all LSMO bulk.	5.77
5.59	The temperature dependence of AC susceptibility for LS <sub>4.0</sub> sample at various applied field.	5.77
5.60	Temperature dependence of resistance for all LSMO bulk.	5.78

5.61	Temperature dependence of resistance for all LSMO thin films.	5.78
5.62	CMR curve of LSMO bulk as a function of magnetic field at various temperatures.	5.79
5.63	CMR curve of all LSMO bulk as a function of temperature at 1 Tesla.	5.79
5.64	CMR curve of LS <sub>4,0</sub> thin film as a function of applied magnetic field at various temperatures.	5.80
5.65	CMR curve of all LSMO thin film as a function of temperatures at 1 Tesla.	5.80
5.66	XRD spectrum for LBMO bulk and ICDD standard.	5.86
5.67	XRD spectrum for all LBMO thin film.	5.87
5.68	Thermal dependence of AC susceptibility at H=10 Oe for all LBMO thin film.	5.87
5.69	Thermal dependence of AC susceptibility at H=10 Oe for LBMO bulk.	5.88
5.70	Inverse AC susceptibility against temperature of LBMO system.	5.88
5.71	The temperature dependence of AC susceptibility for LB <sub>4,0</sub> sample at various applied field.	5.89
5.72	Temperature dependence of resistance for LBMO bulk.	5.89
5.73	Temperature dependence of resistance for all LBMO thin film.	5.90
5.74	Deposition time dependence of T <sub>p</sub> for La-Ba-Mn-O thin films.	5.90
5.75	CMR curve of all LBMO bulk sample as a function of applied magnetic field at various temperature.	5.91
5.76	CMR curve of all LBMO bulk as a function of temperature at 0.1 and 1 Tesla.	5.91

**LIST OF PLATES**

<b>Plates</b>		<b>Pages</b>
4.1	The ESM100 Edward Rf magnetron sputtering system	4.3
4.2	Carbolite box furnace	4.7
4.3	Carbolite double tube furnace	4.9
4.4	Pulsed Laser Deposition system	4.10
4.5	Rotational target holder	4.11
4.6	Handy YAG Lasers (model: HYL 101 E)	4.12
4.7	Focus lens for the PLD system	4.13
4.8	Vacuum system for the Pulsed Laser Deposition	4.14
4.9	Stainless steel substrate holder embedded with heating rod	4.16
4.10	Rotational target holder	4.16
4.11	Target and substrate holder	4.17
4.12	Philips X-ray diffraction unit	4.25
4.13	Lakeshore AC Susceptometer (Model 7000)	4.28
4.14	Four-point probe system for resistance measurement	4.30
4.15	Magnetoresistance measurement system	4.32
5.1	VPSEM micrograph of one of the AgFeCo samples.	5.2
5.2	Low quality GMR granular film	5.2



**LIST OF ABBREVIATIONS/NOTATIONS OF TERMS**

DC	Direct current
RF	Radio frequency
S	Sputtering yield
YAG	Yttrium Aluminium Garnet
PLD	Pulsed Laser Deposition
$L_s$	Distance target to holder
LIPSS	laser-induced periodic surface structures
$\Delta L/L_0$	Thermal expansion
E	Young's modulus
$T_m$	Thermal shocks
$T_{sub}$	Substrate temperature
$T_{cry}$	Crystallization temperature
$T_{epi}$	Epitaxial temperature
MR	Magnetoresistance
OMR	Ordinary Magnetoresistance
AMR	Anisotropic Magnetoresistance
GMR	Giant Magnetoresistance
CMR	Colossal Magnetoresistance
TMR	Tunnelling Magnetoresistance
MBE	Molecular Beam Epitaxy
CIP	current parallel to the plane
CPP	current perpendicular to the plane